Multiplicity dependence of the entropy and heat capacity for pp collisions at LHC energies

C. E. Munguía López, D. Rosales Herrera, A. F. Alvarado García, A. Fernández Téllez, and J. E. Ramírez, tambér de la Ramírez A. Fernández Téllez, and J. E. Ramírez, tambér de la Ramírez A. Fernández Téllez, and J. E. Ramírez.

 ¹Facultad de Ciencias Físico Matemáticas, Benemérita Universidad Autónoma de Puebla, Apartado Postal 165, 72000 Puebla, Pue., México
²Centro de Agroecología, Instituto de Ciencias, Benemérita Universidad Autónoma de Puebla, Apartado Postal 165, 72000 Puebla, Pue., México

We investigate the multiplicity dependence of the transverse momentum spectrum of the charged particle production in pp collisions at LHC energies. To this end, we consider the experimental data sets classified with different multiplicity estimators, defined by the ALICE Collaboration, that are analyzed within the framework of nonextensive particle production. We compute the variance, kurtosis, Shannon entropy, and heat capacity of the p_T spectrum to study the hardening process as a function of the multiplicity and temperature under the different event classifiers. We found that both the Shannon entropy and the heat capacity show different responses for the triggers at the forward-backward and midrapidity regions. We emphasize that the selection of event biases may induce different responses in estimating theoretical and phenomenological observables that could lead to misleading conclusions.

I. INTRODUCTION

The study of particle production in ultrarelativistic collisions provides insights into the physical phenomena occurring at very high energies, pressures, and temperatures [1–5]. The transverse momentum spectrum of the produced particles is a specific experimental measure used to extract or infer information about the system created after the collision and its evolution [6–12]. Fundamentally, the p_T spectrum is a histogram built from the particles' yield observed after the freeze-out hadronic phase. It contains information about the particle production and its underlying physics [13–18].

Over time, various theoretical and phenomenological approaches have been developed to describe the p_T spectrum based on different assumptions encompassing both perturbative and non-perturbative QCD. For instance, the factorization theorem, collinear factorization, parton distribution and fragmentation functions [19], parton-hadron duality [20, 21], and multiple parton interactions [22], among others. In particular, we focus on those founded on statistical physics of large fluctuations to describe the experimental data [23].

One of the earliest approaches to describe the p_T spectrum data of the charged particle production was a p_T -exponential, which resembles the Boltzmann distribution [24–26]. In this approach, the inverse of the decay constant is identified as the effective temperature of the medium formed after the collision [27, 28]. Even though the p_T -exponential captures the experimental behavior of the p_T spectrum data for pp collisions at very low center of mass energies or in the low p_T limit, it fails to describe the hard part of the p_T spectrum, which sub-

stantially deviates from the data as the center of mass energy grows. The latter inspired several authors to introduce quasi-power law functions to describe the p_T spectrum [23, 29, 30]. In particular, the Hagedorn's proposal stands out above all of them because it is a QCD-inspired function that appropriately describes the asymptotic limits of the p_T spectrum observed experimentally [23]. The Hagedorn function behaves as a p_T -exponential function at low p_T and incorporates the power law trend at high p_T values. Later, the high energy particle physics community adopted Tsallis q-exponential functions as generalizations of the p_T -exponential distribution [31–36], having a good performance in fitting the experimental p_T spectrum data, leading to infer information about the systems created in ultrarelativistic particle collisions [37]. However, it is phenomenologically equivalent to the Hagedorn function [38, 39].

Another approach comes from the color string models, which are frameworks frequently used to study the particle production through the fragmentation of color strings stretched between the colliding partons [40]. One way to describe the transverse momentum spectrum of the produced particles is by incorporating the Schwinger mechanism [41] together with string tension fluctuations. For instance, the thermal distribution can be obtained by assuming a Gaussian description for the string tension fluctuations [42]. Nevertheless, heavy-tailed distributions should be considered in order to obtain a p_T spectrum with adequate asymptotic limits: thermal distribution and a power-law tail at low and high p_T values, respectively [43]. This consideration leads to a nonextensive description of the particle production and the medium formed in the collision system, marking the departure from the thermal description [36, 44, 45].

One way to study the processes involved in the charged particle production is by analyzing the p_T spectra under different event classifications. This can be done by computing the Shannon entropy for the normalized p_T spectrum. For instance, in Ref. [45], the authors com-

^{*} diana.rosales.herrera@cern.ch

[†] j.ricardo.alvarado@cern.ch

[‡] jhony.eredi.ramirez.cancino@cern.ch

puted the Shannon entropy for the p_T spectrum of the produced charged particles in minimum bias pp collisions as a function of the center of mass energy (\sqrt{s}) . It was found that the Shannon entropy increases as a function of \sqrt{s} . The latter is expected not only because of the increase in the production of soft particles (which increases the temperature of the medium) but also because of the hardening of the p_T spectrum (greater production of high p_T particles).

In this work, we aim to analyze the multiplicity dependence of the Shannon entropy and heat capacity of the p_T spectrum for the charged particles produced in pp collisions at $\sqrt{s} = 5.02$, 7, and 13 TeV, considering the ALICE V0M and SPD multiplicity classifiers [46, 47]. To this end, we adopt the nonextensive particle production approach, considering the Schwinger mechanism with heavy-tailed string tension fluctuations to describe the p_T spectrum data. One consequence of this approach is that the particle production departs from the thermal equilibrium [36].

We consider the normalized p_T spectrum as a probability density function to compute its moments and the Shannon entropy. The latter is useful to study the dependence of the p_T spectrum on the multiplicity classifiers. Variations are expected since the V0M and SPD classifications are defined from the detectors' signals allocated at two complementary regions, forward-backward and midrapidity, respectively.

The forward-backward region is sensitive to initial collision scatters and long-range correlations, providing information about the longitudinal fragmentation process and the structure of the colliding particles [48]. It is important to note that this region is used to determine the centrality of events in heavy-ion collisions using the Glauber model [49]. Additionally, the ALICE Collaboration uses the V0M multiplicity estimator as a strategy that may minimize the possible auto-correlations induced by using the midrapidity estimator [47, 50]. For instance, the transverse jet fragmentation and event multiplicity may be correlated because they are measured within the same rapidity interval [51]. In contrast, the multiplicity estimator defined in the midrapidity region mainly captures the information of particles created in earlier stages of the medium formed in the collision, which is useful for studying its properties [15, 17].

We emphasize that this manuscript is focused on studying the evolution of the p_T spectrum across multiplicity classes, highlighting the entropy and heat capacity responses in each event classifier.

The rest of the paper is organized as follows. In Sec. II, we discuss the derivation of the p_T spectrum from a nonextensive particle production perspective. In Sec. III, we comment on the methodology and results of the fits to the experimental data for different energies and multiplicity classes. We also discuss the correlations between model parameters and their temperature dependence. In Sec. IV we compute the n-th moments of the p_T spectrum. In Sec. V, we show the results of the Shannon

entropy and the heat capacity of the analyzed p_T spectrum data. A discussion on the physical interpretation of our finding is included in Sec. VI. Finally, we wrap up this work with our concluding remarks and perspectives in Sec. VII.

II. NONEXTENSIVE ORIGIN OF THE TRANSVERSE MOMENTUM SPECTRUM

In string models, the particle production in ultrarelativistic collisions is basically based on the fragmentation of the color strings stretched between the partons in the colliding projectiles. In this way, the transverse momentum of the produced particles is modeled by the Schwinger mechanism [41], given by

$$\frac{dN}{dp_T^2} \propto e^{-\pi p_T^2/x^2},\tag{1}$$

where dN/dp_T^2 denotes the p_T spectrum. Equation (1) can be interpreted as the probability of producing a particle with transverse momentum p_T coming from the fragmentation of a color string with tension x^2 . In a general scenario, the string tension may fluctuate [42–44]. Then, the p_T spectrum should be computed as the following marginal probability

$$\frac{dN}{dp_T^2} \propto \int_0^\infty e^{-\pi p_T^2/x^2} P(x) dx,\tag{2}$$

where P(x) is the probability distribution function for the string tension fluctuations.

It has been shown that the Schwinger mechanism convoluted with a heavy-tailed distribution for the string tension fluctuations gives an adequate description for particle production in pp collisions [43–45]. The main implication of this approach is that the high p_T particle production requires a nonextensive description of the initial state, and then, the medium formed is no longer thermal [36]. These phenomena can be well-modeled by using the q-exponential function, given by [52]

$$e_q(x) = [1 + (1-q)x]^{1/(1-q)}.$$
 (3)

In particular, if P(x) is a q-Gaussian distribution [53]

$$P(x) = \mathcal{N}_q e_q \left(-x^2 / 2\sigma^2 \right), \tag{4}$$

where \mathcal{N}_q is the normalization constant, Eq. (2) becomes

$$\frac{dN}{dp_T^2} \propto U(a, 1/2, z_0 p_T^2),\tag{5}$$

with $a = \frac{1}{q-1} - \frac{1}{2}$ and $z_0 = \pi(q-1)/2\sigma^2$ [43]. In (5), U denotes the confluent hypergeometric function (also known as the Tricomi's function), defined as

$$U(a,b,z) = \frac{1}{\Gamma(a)} \int_0^\infty e^{-zt} t^{a-1} (1+t)^{b-a-1} dt.$$
 (6)

Remarkably, the Tricomi's function (5) has the appropriate asymptotic behaviors observed experimentally. At low p_T values, Eq. (5) recovers the thermal distribution $dN/dp_T^2 \propto e^{-p_T/T_U}$. We adopt the use of the inverse of the constant decay as the soft scale of the p_T spectrum, usually interpreted as an effective temperature, given by

$$T_U = \frac{B(a, 1/2)}{\sqrt{4\pi z_0}},$$
 (7)

where B is the beta function. T_U can be understood as the temperature linked to the p_T spectrum, computed over the ensemble of collision events occurring under the same biases [44]. We must emphasize that the thermal distribution is also obtained from the Schwinger mechanism by assuming Gaussian fluctuations of the string tension [42], which is also recovered by taking the limit $q \to 1$ in the q-Gaussian distribution (4). Another limit of interest occurs when p_T takes high values. In this limit, Eq. (5) becomes the following power law $dN/dp_T^2 \propto (p_T^2)^{\frac{1}{2}-\frac{1}{q-1}}$. Note that q modulates the exponent of the p_T spectrum tail. In this way, larger qvalues mean bigger production of high p_T particles and the hardening of the p_T spectrum. In particular, for the production of charged particles in minimum bias pp collision, it was found that q consistently grows with the center of mass energy [45].

As we commented in the introduction section, the Hagedorn function represents an alternative approach for describing the p_T spectrum data of charged particle production [23, 24, 54], and its phenomenology is equivalent to the Tsallis q-exponential distribution [34, 38] which is given by [55–57]

$$\frac{dN}{dp_T^2} \propto e_{q_e} \left(-p_T/T_e \right),\tag{8}$$

where q_e and T_e are parameters related to the nonextensivity and the soft scale of the system's final state, respectively. Here, we introduce the subscript e to distinguish these parameters from other instances of q used in the context of q-Gaussian string tension fluctuations. The mapping between the Hagedorn function $dN/dp_T^2 \sim (1+p_T/p_0)^{-m}$ and Eq. (8) is the following: $p_0 = mT_e$, and $m = 1/(q_e - 1)$. At low p_T , Eq. (8) behaves as a thermal distribution, with T_e being the inverse of the decay constant. At high p_T , it follows a power-law $\sim p_T^{1/(1-q_e)}$. Similar to the confluent hypergeometric function U, the Tsallis distribution also matches the asymptotic behaviors observed experimentally.

Interestingly, Wilk and Włodarczyk expressed the Tsallis distribution as the convolution of the thermal distribution with nonlocal temperature fluctuations (\mathcal{T}) [31], which is useful to derive the string tension fluctuations $P_e(x)$ associated with Eq. (8). Since the thermal distribution is obtained by the convolution of the Schwinger mechanism with Gaussian string tension fluctuations, $P_e(x)$ can be derived by convoluting the Gaus-

sian distribution with \mathcal{T} [36]. Therefore

$$e_{q_e}(-p_T/T_e) = \int_0^\infty e^{-\pi p_T^2/x^2} P_e(x) dx,$$
 (9)

where $P_{\rm e}(x)$ is given by

$$P_{e}(x) = \frac{1}{\pi T_{e}} \left[\frac{4a_{e}^{2}\pi T_{e}^{2}}{q_{e}^{2}x^{2}} \right]^{a_{e}} U\left(a_{e}, \frac{1}{2}, \frac{4a_{e}^{2}\pi T_{e}^{2}}{q_{e}^{2}x^{2}}\right), \quad (10)$$

with $a_e = q_e/2(q_e - 1)$. For small x, $P_e(x)$ approximates to $\exp[-x^2(2q_e^2 - q_e)/2\pi T_e^2]$. In contrast, for large x, $P_e(x) \sim x^{-2a_e}$. In consequence, $P_e(x)$ is a heavy-tailed distribution [36].

We remark that the U function (5) is derived by considering that the string tension fluctuations obey a q-Gaussian distribution, which is a nonextensive description of the initial state. In contrast, the Tsallis qexponential distribution is, a priori, proposed to describe the p_T spectrum based on the nonthermal arguments of the final state. Interestingly, as we discussed, both approaches can be derived from heavy-tailed distributions for the string tension fluctuations. In this context, the emergence of a heavy-tailed p_T spectrum implies the existence of phenomena out of thermal equilibrium, a necessary requirement for the production of high p_T particles [36, 44, 45]. This connection suggests that nonextensive statistical physics provides a framework for describing a wide range of effects in high-energy collisions, whether through the fragmentation of color strings or temperature fluctuations.

In Sec. III, we analyze the characteristics of the q-exponential distribution and the U function in describing the p_T spectra, categorized by V0M and SPD multiplicity classes in pp collisions, and provide a correlation between the model parameters of both approaches.

III. DATA ANALISYS

We analyze the experimental p_T spectrum data of the charged particle production in pp collisions reported by the ALICE Collaboration at midrapidity using the V0M and SPD multiplicity classes.

Table I. Description of the experimental p_T spectrum data of the charged particle production in pp collisions analyzed in this manuscript. The data is reported by the ALICE Collaboration at midrapidity, classified according to the V0M and SPD definitions at different center of mass energies.

Data set	Rapidity cut	p_T range	Ref.
V0M at 5.02 GeV	$ \eta < 0.8$	0.15 20 GeV	[47]
SPD at 5.02 GeV	$ \eta < 0.8$	$0.15\text{-}20~\mathrm{GeV}$	[47]
V0M at $7 TeV$	$ \eta < 0.5$	$0.16\text{-}40~\mathrm{GeV}$	[46]
V0M at 13 TeV	$ \eta < 0.8$	$0.15\text{-}20~\mathrm{GeV}$	[47]
SPD at 13 TeV	$ \eta < 0.8$	$0.15\text{-}20~\mathrm{GeV}$	[47]

In Table I, we provide detailed information on the kinematic cuts of each data set. We fit Eqs. (5) and (8) to

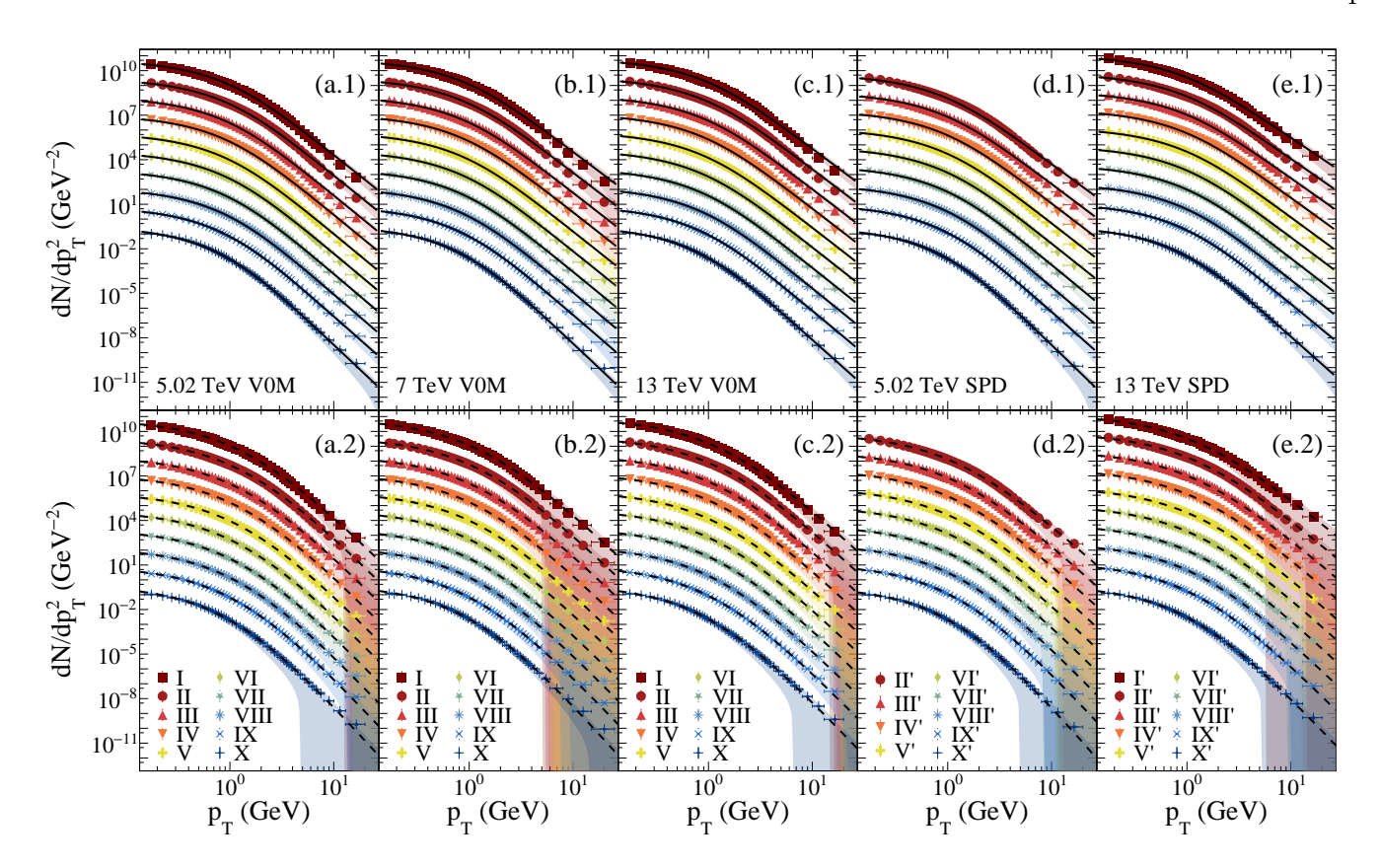


Figure 1. Experimental data of p_T spectrum (markers) of the charged particle production in pp collisions at different center of mass energies under the V0M and SPD classifiers defined by the ALICE Collaboration: (a.1)-(a.2) $\sqrt{s} = 5.02$ TeV (V0M), (b.1)-(b.2) $\sqrt{s} = 7$ TeV (V0M), (c.1)-(c.2) $\sqrt{s} = 13$ TeV (V0M), (d.1)-(d.2) $\sqrt{s} = 5.02$ TeV (SPD), and (e.1)-(e.2) $\sqrt{s} = 13$ TeV (SPD). See Table I for detailed information on the kinematic cuts of the data sets. The solid lines correspond to the fits to data performed via Eq. (5) (top panels) and the dashed lines correspond to the fits using Eq. (8) (bottom panels). In all cases, the shaded region corresponds to the 2- σ uncertainty propagation.

the entire p_T range reported experimentally using the ROOT 6 software. In Fig. 1, we show the fits to the p_T spectrum data. In all cases, the ratio χ^2/NDF takes values around 1, meaning that both approaches provide a good description of the experimental data for all the p_T range reported. However, the error propagation via the model parameters is much better controlled by Eq. (5), as seen in Fig. 1. In all cases, we assumed that the fitting parameters are independent.

We found that the nonextensivity parameters are linearly correlated by $q_e = \lambda_q q + b_q$ with $\lambda_q = 0.53(1)$ and $b_q = 0.46(1)$ (see Fig. 2 (a)), which is consistent with previous parametrizations [36]. On the other hand, the model temperatures follow $T_e = \lambda_T T_U$ with $\lambda_T = 0.868(1)$ (see Fig. 2 (b)).

Additionally, the temperature T_U is a monotonically increasing function of the average multiplicity density (μ) , as seen in Fig. 3 (a). Therefore, it is possible to use T_U as the main natural variable. In all cases, σ and q increase with the multiplicity, and then, with T_U (see Figs. 3 (b) and 4).

Moreover, σ follows a global trend given by

$$\sigma(T_U) = a_{\sigma} T_{II}^{c_{\sigma}},\tag{11}$$

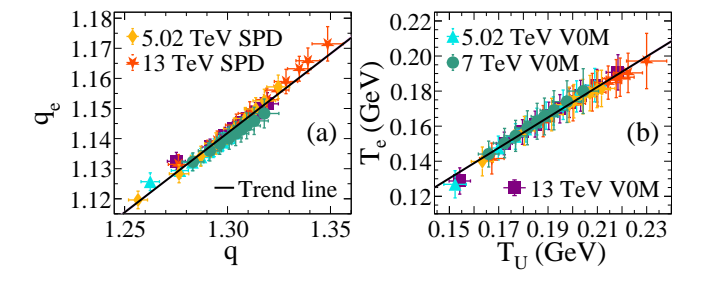


Figure 2. Correlations between the model parameters (a) q_e as a function of q and (b) T_e as a function of T_U for all the analyzed cases. The solid lines correspond to the linear trends.

where $c_{\sigma} = 0.868(1)$ and $a_{\sigma} = 1.94(2)$ GeV^{1-c_{\sigma}}. Relation (11) is valid for all the analyzed data, as shown in Fig. 3 (b).

Figure 4 shows the dependence of q as a function on the temperature for different center of mass energies and multiplicity classifiers. We also propose the following parametrization

$$q(T_U) = q_0 + a_q (T_U - T_0)^{c_q}, (12)$$

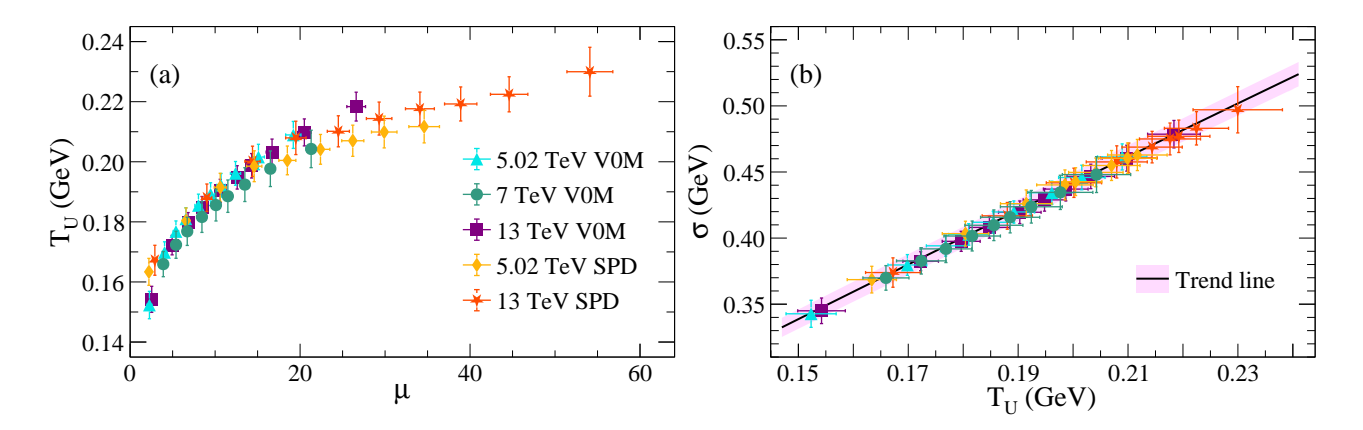


Figure 3. (a) Temperature as a function of the average multiplicity and (b) σ as a function of temperature for all the analyzed data sets. The solid line corresponds to Eq. (11). The shaded region corresponds to the uncertainty propagation.

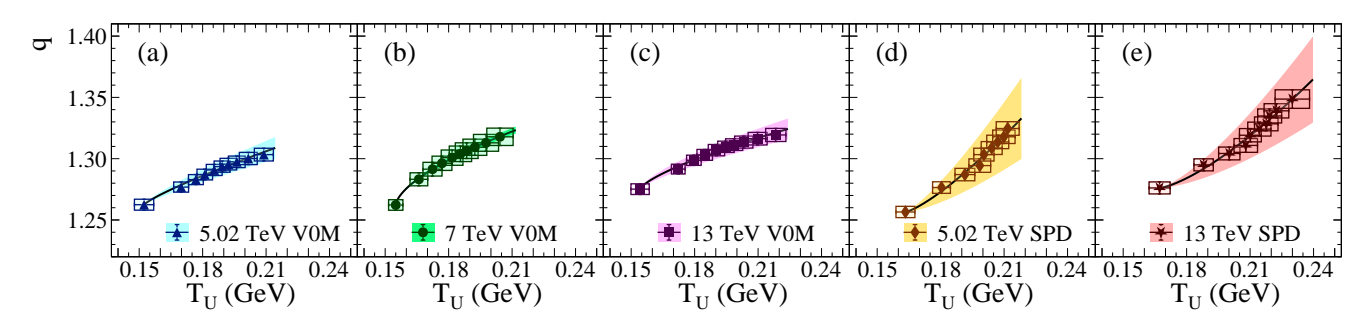


Figure 4. Dependence of the q on the temperature for: (a) $\sqrt{s} = 5.02$ TeV (V0M), (b) $\sqrt{s} = 7$ TeV (V0M), (c) $\sqrt{s} = 13$ TeV (V0M), (d) $\sqrt{s} = 5.02$ TeV (SPD), and (e) $\sqrt{s} = 13$ TeV (SPD). The markers correspond to the fitted value of each data set. The solid lines correspond to the parametrization in Eq. (12). The shaded regions correspond to the uncertainty propagation.

where q_0 and T_0 are the minimal values of q and T_U , corresponding to the lowest multiplicity class of each estimator. The obtained values of a_q and c_q are reported in Table II.

Table II. Values obtained of the relation q vs T_U in Eq. (12).

$\sqrt{s} \; (\text{TeV})$	Classifier	$a_q \; (\mathrm{GeV}^{-c_\sigma})$	c_q
5.02	V0M	0.47 ± 0.07	0.83 ± 0.05
7	V0M	0.37 ± 0.01	0.63 ± 0.01
13	V0M	0.33 ± 0.04	0.72 ± 0.04
5.02	SPD	3.24 ± 1.04	1.29 ± 0.10
13	SPD	3.38 ± 1.02	1.39 ± 0.10

Equation (12) captures some dissimilarities between the multiplicity classifiers through the dependence of qon the temperature. For instance, for the V0M classes, qexhibits a concave-down increasing behavior with T_U (see Figs 4 (a)-(c)), which leads to an apparent saturation of q as the multiplicity increases. This means that there is no substantial increment in the production of high p_T particles in the midrapidity region when the V0 activity grows. In contrast, for the SPD classifier, q exhibits a concave-up increasing behavior with T_U , as shown in Figs 4 (d)-(e). This means that an increase in the multiplicity brings an increment in the production of high p_T particles. The last observation is consistent with the p_T auto-correlation biases implicitly present in the SPD classifier, because the multiplicity classification is determined in the same region where the p_T spectrum is measured [46], as we commented before.

IV. MOMENTS AND STATISTICS OF THE TRANSVERSE MOMENTUM SPECTRUM

The statistical moments of the p_T spectrum provide characteristics on the central tendency, dispersion, and contribution of the tail to the whole spectrum, obtaining insights into the evolution of the p_T spectrum as a function of the average multiplicity.

We compute the n-th moments of the normalized p_T spectrum as follows

$$\langle \mathcal{P}_T^n \rangle = \frac{\int p_T^n \frac{dN}{dp_T^2} dp_T}{\int \frac{dN}{dp_T^2} dp_T}.$$
 (13)

By computing the integral from 0 to infinity, Eq. (13)

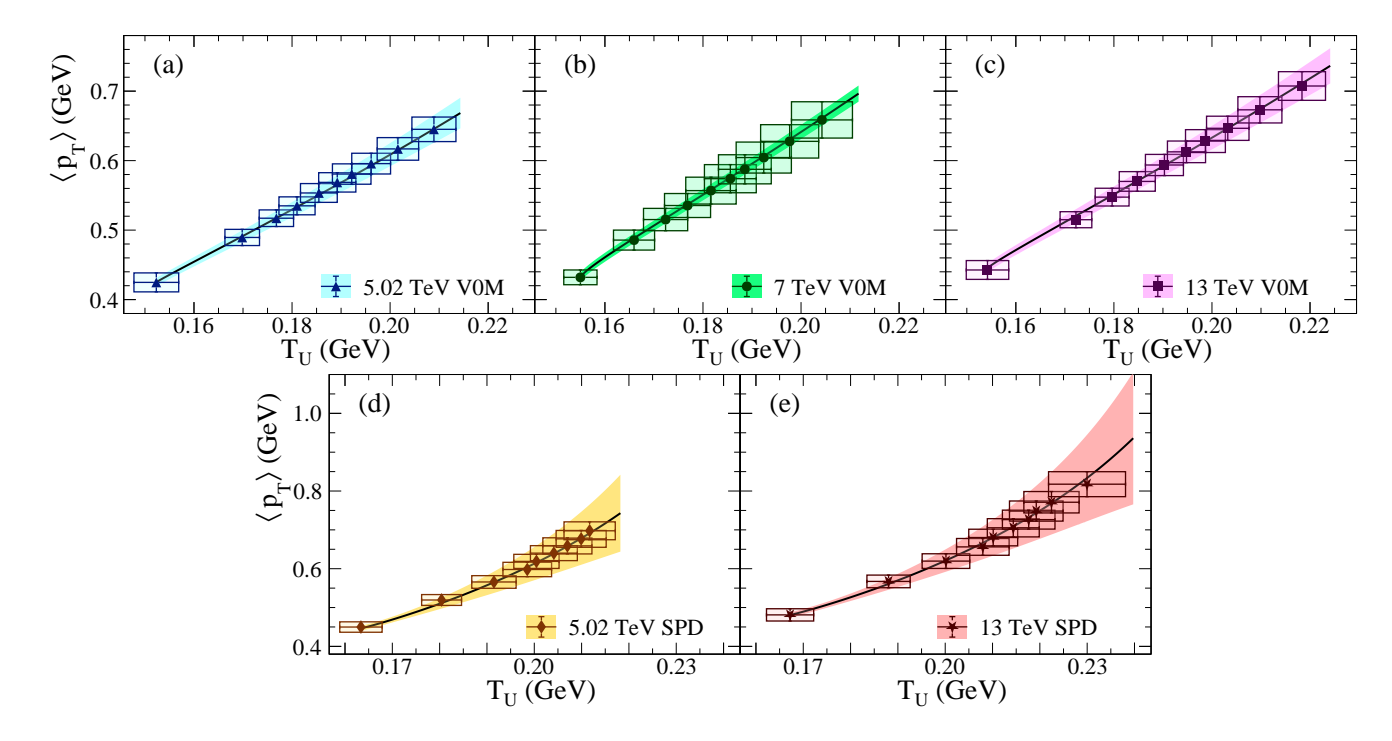


Figure 5. Temperature dependence of the mean p_T (Eq. (16)) of the charged particles produced in pp collisions at (a) $\sqrt{s} = 5.02$ TeV (V0M classes), (b) $\sqrt{s} = 7$ TeV (V0M classes), (c) $\sqrt{s} = 13$ TeV (V0M classes), (d) $\sqrt{s} = 5.02$ TeV (SPD classes), and (e) $\sqrt{s} = 13$ TeV (SPD Classes). The markers correspond to the computed values using the values of q and σ for each data set. The solid lines correspond to the parametrization considering the temperature dependence of q and σ via Eqs. (11) and (12)). The shaded regions correspond to the uncertainty propagation.

can be expressed in the following closed form

$$\langle \mathcal{P}_T^n \rangle = \pi^{\frac{n-1}{2}} 2^n \Gamma\left(\frac{n+1}{2}\right) \left(\frac{2-q}{q-1}\right) \times \frac{B\left(\frac{n+2}{2}, \frac{1}{q-1} - \frac{n+2}{2}\right)}{B\left(\frac{1}{q-1} - \frac{1}{2}, \frac{1}{2}\right)^n} T_U^n, \tag{14}$$

which is well-defined for q < (4+n)/(2+n) [45].

Additionally, the computation of the moments reported by the experiments requires multiplying the factor $2\pi p_T$ from phase space to the p_T spectrum [23]. Thus, we found

$$\langle p_T^n \rangle = \langle \mathcal{P}_T^{n+1} \rangle / \langle \mathcal{P}_T \rangle.$$
 (15)

It is important to emphasize that Eq. (13) can also be computed over the p_T range reported experimentally, which is a kinematic cut defined by the setup where the experiments have an optimal resolution. In those cases, our estimations match the data reported by the experiments, as discussed in Ref. [45].

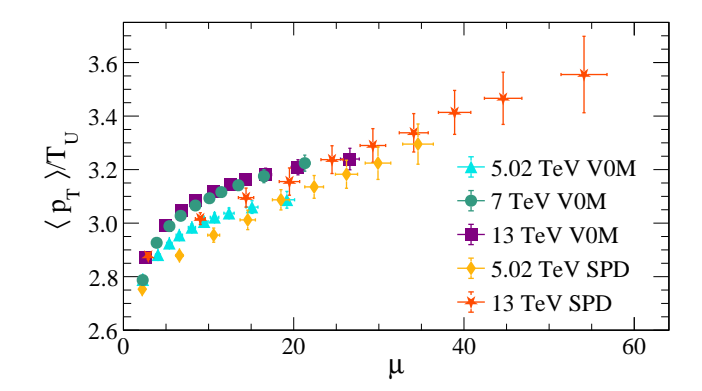


Figure 6. $\langle p_T \rangle / T_U$ as a function of μ for all the analyzed data sets

A. Average transverse momentum

We calculate the mean transverse momentum by setting n=1 in Eq. (15), resulting in

$$\langle p_T \rangle = \frac{(q-1)(3q-5)}{(2-q)(2q-3)} \left(\frac{\Gamma\left(\frac{1}{q-1}\right)}{\Gamma\left(\frac{1}{q-1} - \frac{1}{2}\right)} \right)^2 T_U.$$
 (16)

Note that $\langle p_T \rangle$ is proportional to T_U , where the proportionality constant only depends on q. In the thermal

limit $q \to 1$, Eq. (16) reduces to $\langle p_T \rangle = 2T_U$, describing a purely thermal system.

In Fig. 5, we show the results of the $\langle p_T \rangle$ as a function of the temperature. In all cases, the $\langle p_T \rangle$ increases as the temperature does. In particular, this increment is more pronounced for the SPD classifier than for the V0M's. We also computed the $\langle p_T \rangle$ trend by considering the q and σ as a function of the temperature given by Eqs. (11) and (12).

We observed that the highest values of $\langle p_T \rangle$ correspond to the systems with the largest multiplicities, for which we found the largest values of q. However, in all cases, we found that q > 1, meaning a non-negligible contribution of the produced particles that come directly from rare events [36]. Those events are taken into account by assuming the nonextensive description of the string tension fluctuations, where strong interactions lead to large momentum transfer, resulting in the high p_T and heavy particle production [36]. This is aligned with other descriptions assuming nonextensivity for describing the systems created in high multiplicity pp collisions [57–59].

In Fig. 6, we show the ratio $\langle p_T \rangle / T_U$ for all the experimental data analyzed, which deviates from 3, the value estimated for the medium form in central heavy ion collision for systems undergoing to a very quick thermalization [60, 61].

B. Variance and kurtosis of the transverse momentum spectrum

The variance of the p_T spectrum is computed in the standard form, $\operatorname{var}(\mathcal{P}_T) = \langle \mathcal{P}_T^2 \rangle - \langle \mathcal{P}_T \rangle^2$, obtaining [45]

$$\frac{\operatorname{var}(\mathcal{P}_T)}{T_U^2} = \frac{2(q-1)}{3-2q} \left[\frac{\Gamma\left(\frac{1}{q-1}\right)}{\Gamma\left(\frac{1}{q-1} - \frac{1}{2}\right)} \right]^2 - \left[\frac{4-2q}{5-3q} \right]^2. \tag{17}$$

We point out that the variance over the square of the temperature is a function of q. Interestingly, this ratio tends to 1 in the thermal limit [45].

It is important to extend the analysis of the p_T spectrum beyond the variance estimation and consider the information from the heavy tail to study the p_T spectrum shape. In particular, the kurtosis measures the contribution of the tails to the total probability, which corresponds to the observation of rare events that dominate the production of high p_T particles. We compute the kurtosis as the fourth standardized moment, defined as

$$\operatorname{kurt}(\mathcal{P}_{T}) = \frac{\left\langle \mathcal{P}_{T} \right\rangle^{4} \left[\frac{\left\langle \mathcal{P}_{T}^{4} \right\rangle}{\left\langle \mathcal{P}_{T} \right\rangle^{4}} - \frac{4\left\langle \mathcal{P}_{T}^{3} \right\rangle}{\left\langle \mathcal{P}_{T} \right\rangle^{3}} + \frac{6\left\langle \mathcal{P}_{T}^{2} \right\rangle}{\left\langle \mathcal{P}_{T} \right\rangle^{2}} - 3 \right]}{\left[\operatorname{var}(\mathcal{P}_{T}) \right]^{2}}. \quad (18)$$

Note that the calculation of $\langle \mathcal{P}_T^4 \rangle$ from Eq. (14) requires 1 < q < 4/3 for a finite estimation of the kurtosis when considering the integration range from 0 to infinity.

This restriction is not presented in the kurtosis computation from the experimental p_T spectrum because it is reported in a limited p_T range.

We remark that in the thermal limit, the kurtosis tends to 9, meaning that the high p_T particle production rate is not affected by increments in the center of mass energy or the multiplicity of the system.

In Fig. 7, we show the behavior of the p_T spectrum variance (top panels) and kurtosis (bottom panels) as a function of the temperature for both the V0M and SPD classifiers at $\sqrt{s}=5.02$, 7 (only V0M), and 13 TeV. In Fig. 7 (bottom panels), we present the kurt(\mathcal{P}_T) as a function of the temperature for all the analyzed datasets. We also consider the parametrization of q and σ in terms of the temperature (see Eqs. (11) and (12)) for estimating the trend of the variance and kurtosis.

Note that the highest multiplicity values are very close to the limit value at which kurtosis diverges. In consequence, there is a substantial increment in the uncertainty propagation in the data sets and the trend lines as shown in Fig. 7 panels (c.2)-(e.2). In fact, for the I' SPD class at 5.02 TeV and the III', II', and I' SPD classes at 13 TeV, the $\langle \mathcal{P}_T^4 \rangle$ is not finite.

In both cases, variance and kurtosis exhibit an increasing trend with the temperature, with a more pronounced concave-up behavior observed for the SPD classification. This indicates that the p_T spectrum becomes flattened at low p_T with an enhancement of the probability of producing high p_T particles as the temperature or the multiplicity increases.

V. DEPENDENCE OF THE SHANNON ENTROPY AND HEAT CAPACITY ON THE MULTIPLICITY CLASSIFIERS

In 1948, C. E. Shannon introduced the quantity $\mathcal{H} =$ $-\langle \ln P(x) \rangle$ as a measure of the information content in a probability distribution describing the random variable x [62]. In Ref. [45], the authors studied the Shannon entropy of the normalized p_T spectrum for the charged particle production in minimum bias pp collisions. The study of the Shannon entropy can provide information regarding the contribution of the soft and hard parts. In particular, for the thermal distribution, the Shannon entropy is $1 + \ln T$ [45]. However, we expect deviations from the latter since the experimental data of the p_T spectrum exhibits a power law tail. In those cases, the increment of the Shannon entropy not only comes from a flattening of the soft part but also increases with an enhancement of the high p_T particle production, which may differ from one event classification to another as a consequence of the selection bias.

We computed the Shannon entropy by considering the normalized p_T spectrum as follows

$$\mathcal{H} = -\int_0^\infty \left(\frac{1}{I_0} \frac{dN}{dp_T^2}\right) \ln \left(\frac{1}{I_0} \frac{dN}{dp_T^2}\right) dp_T, \quad (19)$$

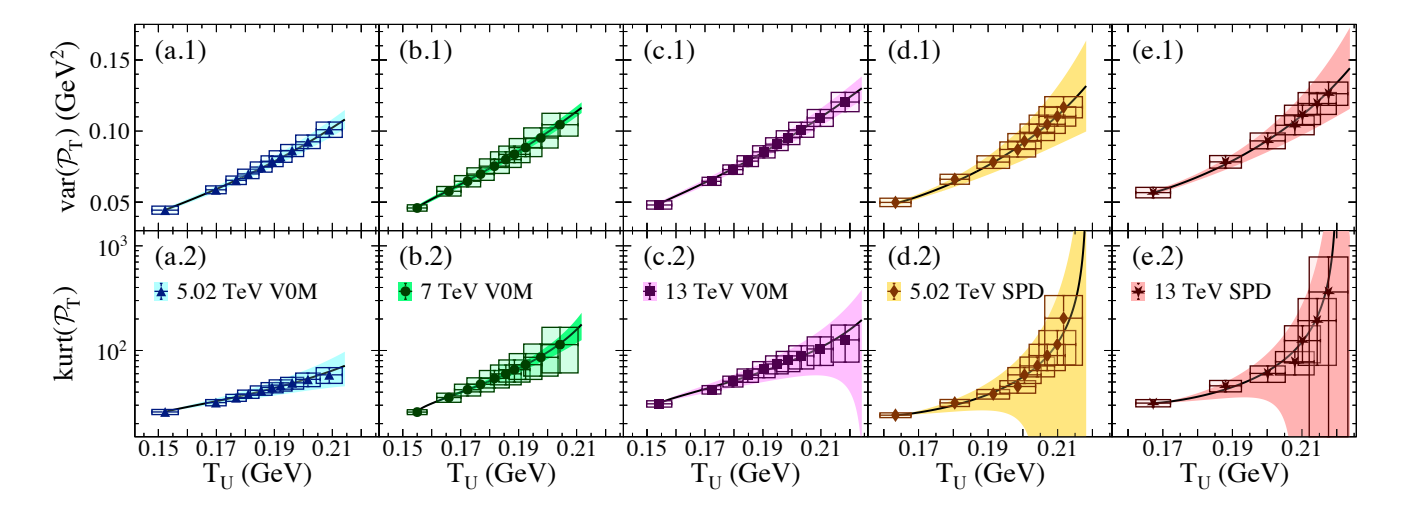


Figure 7. Temperature dependence of variance (top panels) , and kurtosis (bottom panels) of the transverse momentum spectrum of the charged particles produced in pp collisions at (a.1)-(a.2) $\sqrt{s} = 5.02$ TeV (V0M classes), (b.1)-(b.2) $\sqrt{s} = 7$ TeV (V0M classes), (c.1)-(c.2) $\sqrt{s} = 13$ TeV (V0M classes), (d.1)-(d.2) $\sqrt{s} = 5.02$ TeV (SPD classes), and (e.4)-(e.2) $\sqrt{s} = 13$ TeV (SPD classes). Lines, figures, and colors are the same as in Fig. 5.

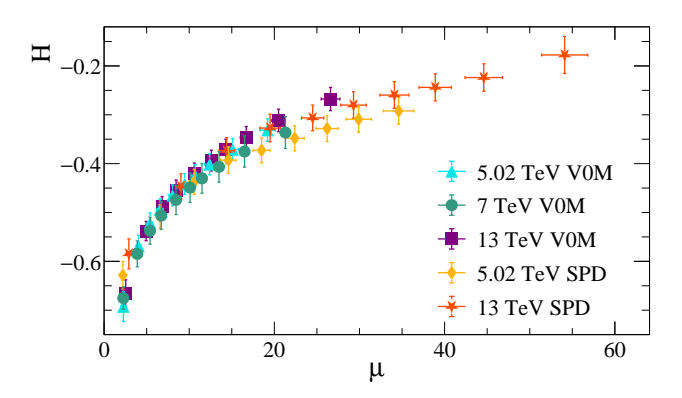


Figure 8. Shannon entropy as a function of the average multiplicity density for all the analyzed data sets.

where

$$I_0 = \int_0^\infty \frac{dN}{dp_T^2} dp_T = \frac{\sigma}{(2-q)\Gamma(a)} \sqrt{\frac{q-1}{2}}$$
 (20)

is the normalization constant of Eq. (5). This marks a natural way of computing Eq. (19) by considering p_T as the random variable, according to what is usually done in the generalized ensemble theory [63, 64]. Since the description of the p_T spectrum through (5) involves the Tricomi's function, the computation of the Shannon entropy must be performed by using numerical methods.

Figures 8 and 9 show our estimations of the Shannon entropy for the p_T spectrum data sets analyzed as a function of the average multiplicity density and the temperature, respectively. In all cases, \mathcal{H} is a monotonically increasing function. In Fig. 8, the Shannon entropy shows very similar behavior for the SPD and V0M classifiers. In contrast, Fig. 9 shows a concave-down increasing behavior with the temperature for the V0M classes, which

is not observed for the SPD classifier.

Note that the increment in the V0M signal corresponds to an increment of the forward-backward activity, which has a nontrivial response in the shape of the p_T spectrum measured in the midrapidity region [50, 65]. On the other hand, for the SPD classifier, the Shannon entropy increases with the multiplicity, which is expected because the SPD classifier is directly defined through the number of tracklets detected in the midrapidity region. Thus, the production of charged particles with high p_T is enhanced as the multiplicity increases, raising the value of q and, therefore, the temperature value.

We also analyze the rate of change of the Shannon entropy as a function of temperature to determine the subtle differences present in the multiplicity classifiers. This is done by computing the heat capacity, which is defined in thermodynamics as follows

$$C = T_U \frac{d\mathcal{H}}{dT_U},\tag{21}$$

which is interpreted as a measure of how much heat is required to warm up the system at which the particles are produced. From the definition of T_U in Eq. (7), the temperature grows with increments of σ and q, but in all cases, it occurs simultaneously as a function of the average multiplicity. In this way, heating the p_T spectrum means a flattening of the soft part (production of soft particles in a larger low p_T region) and an enhancement of the p_T spectrum tail (higher rate of producing high p_T particles).

The computation of the heat capacity (21) demands knowing the explicit or implicit dependence of the Shannon entropy on the temperature. To do this, we use the explicit dependence of σ and q as a function of T_U , given by Eqs. (11) and (12), respectively. In general, the heat capacity can not be expressed as a closed formula

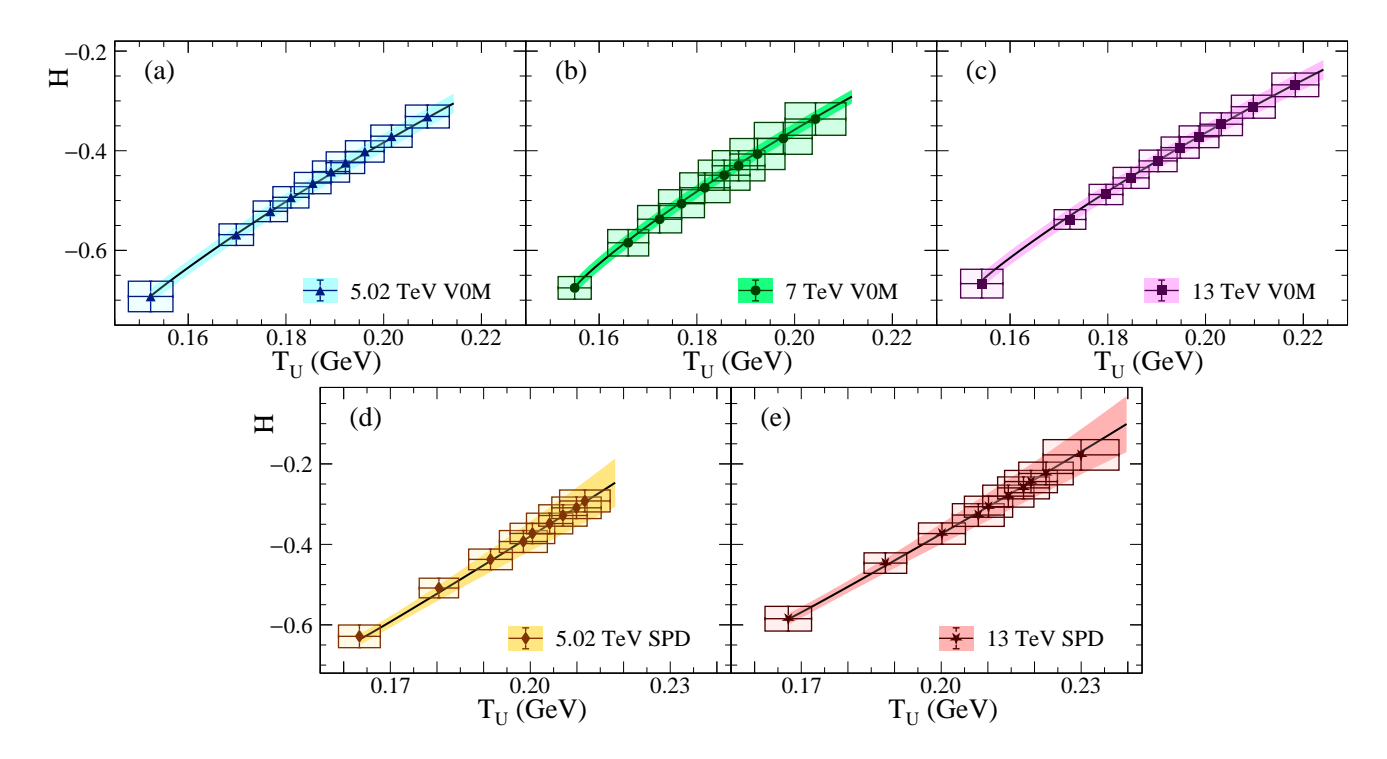


Figure 9. Shannon entropy as a function of the temperature for: (a) $\sqrt{s} = 5.02$ TeV (V0M), (b) $\sqrt{s} = 7$ TeV (V0M), (c) $\sqrt{s} = 13$ TeV (V0M), (d) $\sqrt{s} = 5.02$ TeV (SPD), and (e) $\sqrt{s} = 13$ TeV (SPD). The markers correspond to the computed values of the Shannon entropy using Eq. (19) for each data set. In all cases, the solid lines correspond to the estimation of \mathcal{H} considering the parametrizations of σ and q in (11) and (12), respectively. The shaded regions correspond to the uncertainty propagation.

for the Tricomi's function (5). In fact, it requires the computation of some derivatives of the U function and the integration of terms of the form $U \ln U'$, as discussed in Ref. [45]. In this way, we also numerically compute the heat capacity for all cases. Figure 10 contains our estimations of the heat capacity for the analyzed data.

We found that the heat capacity is sensitive to the multiplicity classifier. The heat capacity for the SPD classification increases as the multiplicity does, as expected. It means the system requires more energetic collisions to produce more charged particles and, at the same time, with higher p_T values. Interestingly, the heat capacity for the V0M classes shows a decreasing concave-up behavior more pronounced for pp collisions at 7 TeV, which could be attributed to the more constrained pseudorapidity cut ($|\eta| < 0.5$). The main implication is that the system demands more energetic collisions to lower the system's temperature, which is opposite to the SPD classifier. This occurs because the V0M classes are defined over distributions of tracklets that are not mutually exclusive. Moreover, the increasing concave-behavior of the q value for the V0M classes is a direct indication that the system produces higher p_T particles with a significantly lower rate as the average multiplicity increases. This behavior impacts the heat capacity at higher temperatures and makes the system less accessible at lowertemperature states.

VI. DISCUSSION

In this manuscript, we have used a nonextensive approach to study how the p_T spectrum of charged particle production evolves with multiplicity in pp collisions. Where the data are categorized using two different multiplicity estimators defined by the ALICE Collaboration: V0M and SPD. The model considers that the p_T spectrum arises from the fragmentation of color strings with heavy-tailed tension fluctuations. In particular, if the string tension fluctuations follow Eqs. (4) and (10), the p_T spectrum becomes the Tricomi function (5) and the Tsallis distribution (8), respectively. Interestingly, both distributions resemble an exponential decay at low p_T , allowing us to define the temperature as the inverse of the decay constant, as usual. On the other hand, the U and Tsallis distributions exhibit power-law tails at the high p_T regime, modulated by q and q_e , respectively. Thus, the increase of the q and q_e values is directly linked to the enhancement of high p_T particle production, which refers to a hardening of the p_T spectrum. Notably, the nonextensive approach accurately described the experimental data across the entire p_T -range, indicating that the majority of the particle production in pp collisions originates from string fragmentation. This is in agreement with the consensus that the collective phenomena have minimal influence on the p_T spectrum in pp collisions [17].

We established the correlation between the tempera-

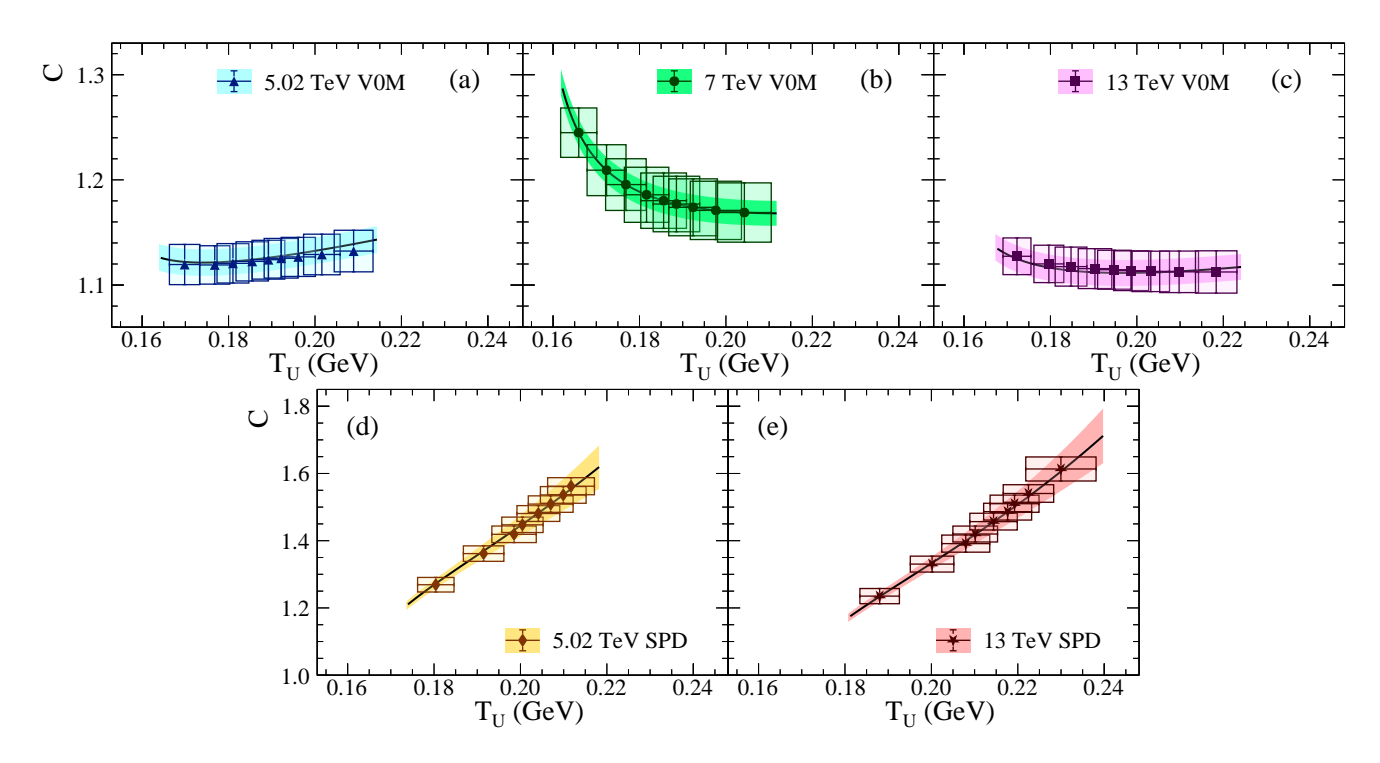


Figure 10. Heat capacity as a function of the temperature for: (a) $\sqrt{s} = 5.02$ TeV (V0M), (b) $\sqrt{s} = 7$ TeV (V0M), (c) $\sqrt{s} = 13$ TeV (V0M), (d) $\sqrt{s} = 5.02$ TeV (SPD), and (e) $\sqrt{s} = 13$ TeV (SPD). The markers correspond to the computed values of the heat capacity using the values of q and σ and the derivative with respect to the temperature of their parametrizations for each data set. In all cases, the solid lines correspond to the estimation of C considering the only parametrizations of q and σ . The shaded regions correspond to the uncertainty propagation.

tures and nonextensivity parameters of both descriptions as part of our analysis. For instance, q_e shows a linear correlation $q=0.53q_e+0.46$, as seen in Fig. 2 (a), although q_e consistently remains below 1.2, within the expected range discussed in Ref. [30]. The soft scales T_U and T_e are proportional, with $T_e=0.87T_U$, as shown in Fig. 2 (b). This is consistent with previous findings showing that $P_e(x)$ has a smaller variance than the q-Gaussian distribution at lower tensions, explaining the underestimation of T_e relative to T_U [36]. Given the correlations discussed above, it was sufficient to carry out the analysis using only the description based on the Tricomi's function.

We observed that, in all the analyzed cases, q increases monotonically with the temperature T_U , as shown in Fig. 4. The latter implies that high p_T particle production is not suppressed, which is consistent with the lack of conclusive evidence of the jet quenching phenomena in pp collisions [17, 66]. This behavior contrasts with that observed in AA collisions, where q decreases with multiplicity, aligned with the suppression of high p_T particles in larger systems [43, 44].

We found significant differences in the dependence of q as a function of T_U across the multiplicity classifiers. For V0M classes, q saturates, indicating a poor enhancement of the hard particle production with increments of the temperature or multiplicity. On the other hand, q is a concave-up function of T_U , meaning the hardening of

the p_T spectrum. This contrast is supported by the definitions of the multiplicity estimators. The classification using the mid rapidity signal (SPD classes) allows for harder spectra at high multiplicities because the tracklets classification can distinguish very high multiplicity events that make classes with high $\langle p_T \rangle$. For instance, the I'-V' classes of SPD of pp collisions at $\sqrt{s} = 13 \text{ TeV}$ contain 1.419% of the total events, while the I class of V0M corresponds to 1% of the events, as the ALICE collaboration reported in Ref. [47]. However, the V0M class I (highest multiplicity) does not necessarily contain information on all the highest multiplicity events in the transverse region. This is because the V0M classes are constituted by tracklet distributions. Consequently, the mean p_T takes smaller values due to the large contribution of low multiplicity events. In contrast, the SPD classification discriminates events with higher multiplicity and, therefore, harder p_T spectra.

We further studied the differences between the V0M and SPD classifiers by analyzing the Shannon entropy as a function of the multiplicity, which was computed by considering the normalized p_T spectrum through the U function (see Eq. (19)). Interestingly, \mathcal{H} increases monotonically with multiplicity. This behavior indicates that the p_T spectrum becomes broader as a consequence of an increment of the temperature (flattening of the p_T spectrum) and the raising of the probability of producing high p_T particles (hardening of the p_T spectrum). However,

the growth of the entropy as a function of temperature differs depending on the event classifier. Similar to q, \mathcal{H} shows signs of saturation for the V0M classes, while for the SPD classes it follows a concave-up increasing behavior.

Due to the different responses of the Shannon entropy as a function of the multiplicity in the different classifiers, we investigated the rate of change of entropy with temperature through the heat capacity, defined in Eq. (21). This methodology allowed us to characterize in more detail the deviations present in the evolution of the p_T spectrum for the V0M and SPD multiplicity classifiers. In the case of the V0M classes, there are temperature intervals where the heat capacity decreases (see top panels of Fig. 10). In particular, for $\sqrt{s} = 7$ TeV, the heat capacity is a monotonically decreasing function of T_U . An explanation for this phenomenon may come from the perspective of an asymmetric relaxation of the system's evolution produced by the event selection biases. In contrast, for the SPD classes, the heat capacity always increases with temperature (see bottom panels of Fig. 10). This is expected because the increments in the number of tracklets in the midrapidity region are directly associated with the high p_T particle production.

The behavior of the heat capacity can be interpreted in the usual thermodynamic sense: An increasing heat capacity indicates that more energy is required to heat up the p_T spectrum, as seen for the SPD classes. In contrast, a decreasing heat capacity reflects that higher-temperature configurations become more accessible than lower-temperature ones, as we obtained for the V0M classes.

VII. SUMMARY AND OUTLOOK

In this work, we studied the dependence on the multiplicity of the average p_T , variance, kurtosis, Shannon entropy, and heat capacity of the p_T spectrum of charged particles produced in pp collisions. To this end, we analyzed the data sets for the center of mass energies of 5.02, 7, and 13 TeV classified under the V0M and SPD multiplicity estimators reported by the ALICE Collaboration (see Table I for detailed information on the kinematic cuts of the analyzed data sets). We fitted the Tricomi's function (5) and the Tasllis distribution (8) to the experimental data of the p_T spectra. We found that the nonextensivity parameters and temperatures of both descriptions are correlated. In particular, we studied the dependence of q and σ on the average multiplicity and

the temperature T_U (given by Eq. (7)). We found that the behavior of q is classifier-dependent: it saturates with V0M but it increases monotonically with SPD without saturation signals. The latter implies a stronger enhancement of hard particle production for the SPD classes.

In the computation of the $\langle p_T \rangle$, the variance, and the kurtosis of the p_T spectrum considering the range from 0 to infinity, we found that all quantities are increasing functions of the temperature T_U and multiplicity, reflecting the increase of the production of particles with higher p_T . In general, the increasing values of the statistics are consequence of the flattening of the soft region along with a lifting of the distribution's tail. All of the above result in an increase in the information content in the entire p_T spectrum as the classes reach higher multiplicities, which was evaluated by computing the Shannon entropy through the normalized p_T spectrum described by the Tricomi's function. In all cases, \mathcal{H} increases with the multiplicity, aligned with a hardening of the p_T spectrum. However, for SPD classes, the Shannon entropy shows an increasing concave-up behavior. Meanwhile, for the V0M classes, the entropy shows an increasing concave-down behavior.

We also estimated the heat capacity as the derivative of the entropy with respect to the temperature (see Eq. (21)). We found different behaviors of the heat capacity as a function of the multiplicity for the V0M and SPD classifiers. In the case of the V0M classes, our analysis revealed that it is easier for the system to get higher temperatures than to cool it down. Meanwhile, for the SPD classes, more energy is required to increase the temperature of the system. We must point out that the multiplicity classifier chosen to select events may induce different responses in estimating theoretical or phenomenological observables that could lead to misleading interpretations or conclusions.

Finally, an immediate extension of this work is the analysis of the p_T spectrum of the changed particle production under different event shape selectors, such as the transverse spherocity, relative transverse activity, or flatenicity, among others.

ACKNOWLEDGMENTS

This work was funded by Consejo Nacional de Humanidades, Ciencias y Tecnologías (CONAHCYT-México) under the project CF-2019/2042, graduated fellowship grant number 1140160, and postdoctoral fellowship grant numbers 645654 and 289198.

^[1] BRAHMS Collaboration, Nucl. Phys. A 757, 1 (2005).

^[2] PHOBOS Collaboration, Nucl. Phys. A **757**, 28 (2005).

^[3] STAR Collaboration, Nucl. Phys. A **757**, 102 (2005).

^[4] PHENIX Collaboration, Nucl. Phys. A **757**, 184 (2005)

^[5] ALICE Collaboration, Eur. Phys. J. C 84, 813 (2024).

^[6] R. Vogt, Ultrarelativistic Heavy-Ion Collisions (Elsevier Science B.V., Amsterdam, 2007) pp. 221–278.

^[7] P. Romatschke and U. Romatschke, Relativistic Fluid Dynamics In and Out of Equilibrium, Cambridge Monographs on Mathematical Physics (Cambridge University

- Press, 2019).
- [8] ALICE Collaboration, Eur. Phys. J. C 73, 2662 (2013).
- [9] ALICE Collaboration, Phys. Lett. B **753**, 319 (2016).
- [10] ALICE Collaboration, JHEP 11, 013 (2018).
- [11] W. Busza, K. Rajagopal, and W. van der Schee, Ann. Rev. Nucl. Part. Sci. 68, 339 (2018).
- [12] ALICE Collaboration, Phys. Lett. B 845, 138110 (2023).
- [13] ALICE Collaboration, Phys. Lett. B **728**, 25 (2014).
- [14] ALICE Collaboration, Phys. Lett. B **760**, 720 (2016).
- [15] CMS Collaboration, Phys. Lett. B **765**, 193 (2017).
- [16] ALICE Collaboration, Nature Phys. 13, 535 (2017).
- [17] J. L. Nagle and W. A. Zajc, Ann. Rev. Nucl. Part. Sci. 68, 211 (2018).
- [18] F. Arleo and G. Falmagne, Phys. Rev. D 109, L051503 (2024).
- [19] J. C. Collins and D. E. Soper, Ann. Rev. Nucl. Part. Sci. 37, 383 (1987).
- [20] G. Veneziano, Nuovo Cim. A 57, 190 (1968).
- [21] J. D. Bjorken and J. B. Kogut, Phys. Rev. D 8, 1341 (1973).
- [22] M. Diehl, D. Ostermeier, and A. Schafer, JHEP 03, 089 (2012), [Erratum: JHEP 03, 001 (2016)].
- [23] R. Hagedorn, Riv. Nuovo Cim. 6N10, 1 (1983).
- [24] R. Hagedorn, Nuovo Cim. Suppl. 3, 147 (1965).
- [25] R. Hagedorn and J. Ranft, Nuovo Cim. Suppl. 6, 169 (1968).
- [26] S. C. Frautschi, Phys. Rev. D 3, 2821 (1971).
- [27] P. Braun-Munzinger, J. Stachel, J. Wessels, and N. Xu, Phys. Lett. B 344, 43 (1995).
- [28] J. C. Texca García, D. Rosales Herrera, J. E. Ramírez, A. Fernández Téllez, and C. Pajares, Phys. Rev. D 106, L031503 (2022).
- [29] C. Michael and L. Vanryckeghem, J. Phys. G 3, L151 (1977).
- [30] T. Bhattacharyya, J. Cleymans, S. Mogliacci, A. S. Parvan, A. S. Sorin, and O. V. Teryaev, Eur. Phys. J. A 54, 222 (2018).
- [31] G. Wilk and Z. Włodarczyk, Phys. Rev. Lett. 84, 2770 (2000).
- [32] G. Bíró, G. G. Barnaföldi, T. S. Biró, and K. Ürmössy, AIP Conf. Proc. 1853, 080001 (2017).
- [33] T. Bhattacharyya, J. Cleymans, L. Marques, S. Mogliacci, and M. W. Paradza, J. Phys. G 45, 055001 (2018).
- [34] K. Saraswat, P. Shukla, and V. Singh, J. Phys. Commum. 2, 035003 (2018).
- [35] P.-P. Yang, F.-H. Liu, and R. Sahoo, Adv. High Energy Phys. 2020, 6742578 (2020).
- [36] D. Rosales Herrera, J. R. Alvarado García, A. Fernández Téllez, J. E. Ramírez, and C. Pajares, Phys. Rev. C 110, 015205 (2024).
- [37] A. N. Mishra, G. G. Barnaföldi, and G. Paić, J. Phys. G 50, 095004 (2023).
- [38] C.-Y. Wong, G. Wilk, L. J. L. Cirto, and C. Tsallis,

- Phys. Rev. D 91, 114027 (2015).
- [39] M. Rybczynski and Z. Włodarczyk, Symmetry 12, 1339 (2020).
- [40] B. Andersson, The Lund model (Cambridge University Press, 1998).
- [41] J. Schwinger, Phys. Rev. 128, 2425 (1962).
- [42] A. Bialas, Phys. Lett. B **466**, 301 (1999).
- [43] C. Pajares and J. E. Ramírez, Eur. Phys. J. A 59, 250 (2023).
- [44] J. R. Alvarado García, D. Rosales Herrera, P. Fierro, J. E. Ramírez, A. Fernández Téllez, and C. Pajares, J. Phys. G Nucl. Partic. 50, 125105 (2023).
- [45] D. Rosales Herrera, J. R. Alvarado García, A. Fernández Téllez, J. E. Ramírez, and C. Pajares, Phys. Rev. C 109, 034915 (2024).
- [46] ALICE Collaboration, Phys. Rev. C 99, 024906 (2019).
- [47] ALICE Collaboration, Eur. Phys. J. C **79**, 857 (2019).
- [48] CMS Collaboration, JHEP **09**, 091 (2010).
- [49] M. L. Miller, K. Reygers, S. J. Sanders, and P. Steinberg, Ann. Rev. Nucl. Part. Sci. 57, 205 (2007).
- [50] ALICE Collaboration, JHEP **09**, 049 (2013).
- [51] A. Ortiz, G. Bencedi, and H. Bello, J. Phys. G 44, 065001 (2017).
- [52] S. Abe, Phys. Rev. E 66, 046134 (2002).
- [53] A. A. Budini, Phys. Rev. E 86, 011109 (2012).
- [54] J. Rafelski, ed., "Thermodynamics of Distinguishable Particles: A Key to High-Energy Strong Interactions?" in Melting Hadrons, Boiling Quarks - From Hagedorn Temperature to Ultra-Relativistic Heavy-Ion Collisions at CERN: With a Tribute to Rolf Hagedorn (Springer International Publishing, Cham, 2016) pp. 183–222.
- [55] A. Bialas, Phys. Lett. B 747, 190 (2015).
- [56] S. Deb, G. Sarwar, R. Sahoo, and J.-e. Alam, Eur. Phys. J. A 57, 195 (2021).
- [57] G. Bíró, G. G. Barnaföldi, and T. S. Biró, J. Phys. G 47, 105002 (2020).
- [58] P. Braun-Munzinger and J. Stachel, Phys. Lett. B 490, 196 (2000).
- [59] M. Badshah, M. Waqas, A. M. Khubrani, and M. Ajaz, EPL 141, 64002 (2023).
- [60] S. Schlichting and D. Teaney, Ann. Rev. Nucl. Part. Sci. 69, 447 (2019).
- [61] F. G. Gardim, G. Giacalone, M. Luzum, and J.-Y. Ollitrault, Nature Phys. 16, 615 (2020).
- [62] C. E. Shannon, Bell Syst. Tech. J 27, 379 (1948).
- [63] R. K. Niven and B. Andresen, in Complex Physical, Biophysical and Econophysical Systems (World Scientific, 2010) pp. 283–317.
- [64] T. Langen, S. Erne, R. Geiger, B. Rauer, T. Schweigler, M. Kuhnert, W. Rohringer, I. E. Mazets, T. Gasenzer, and J. Schmiedmayer, Science 348, 207 (2015).
- [65] G. Nijs and W. van der Schee, Phys. Lett. B 853, 138636 (2024).
- [66] ALICE Collaboration, JHEP **05**, 229 (2024).